Understanding Formation and Roles of Ni^{II} Aryl Amido and Ni^{III} Aryl Amido Intermediates in Ni-Catalyzed Electrochemical Aryl Amination Reactions

Jian Luo,[a] Michael T. Davenport,[b] Chad Callister,[a] Shelley D. Minteer,[c] Daniel H. Ess,[*b] and T. Leo Liu[*a]

a. Department of Chemistry and Biochemistry, Utah State University, Logan, Utah 84322

b. Department of Chemistry and Biochemistry, Brigham Young University, Provo, Utah 84604

c. Department of Chemistry, University of Utah, Salt Lake City, Utah, 84112

Corresponding: dhe@chem.byu.edu, leo.liu@usu.edu

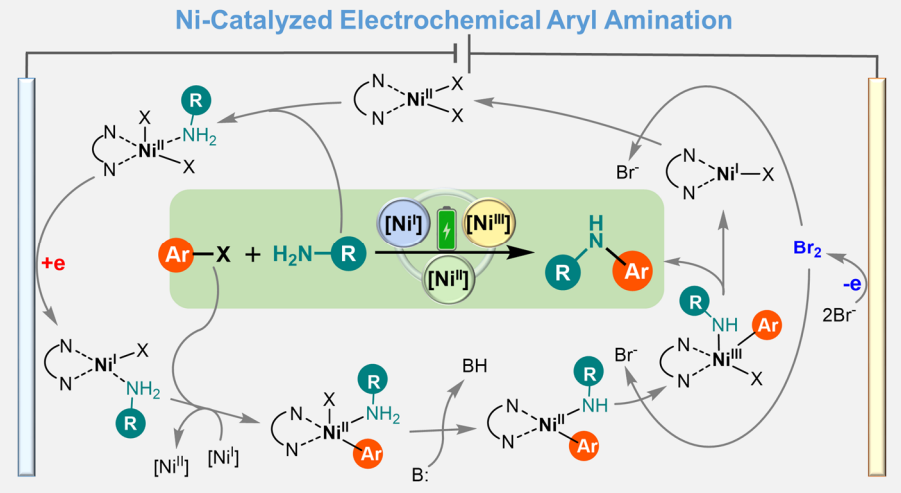

Abstract: Ni-catalyzed electrochemical aryl amination (e-amination) is an attractive, emerging approach to forging C–N bonds as it uses air-stable Ni catalysts and efficiently proceeds at room temperature. However, in-depth mechanistic understandings of this new C–N cross-coupling methodology remain underexplored. Herein, extensive experimental and computational studies were conducted to examine the mechanism of Ni-catalyzed electrochemical aryl amination reactions. The results suggest coordination of an amine to the Ni^{II} catalyst occurs before the cathodic reduction and oxidative addition steps. A stable Ni^{II} aryl amido intermediate is produced from the cathodic half-reaction, a critical step in controlling the selectivity between cross-coupling and undesired homo-coupling reaction pathways. In addition, redox-active bromide in the supporting electrolyte functions as a redox mediator to promote the oxidation of the stable Ni^{II} aryl

amido intermediate to a Ni^{III} aryl amido intermediate. Subsequently, the Ni^{III} aryl amido intermediate undergoes facile reductive elimination to provide a C−N cross-coupling product at room temperature. These mechanistic insights about the Ni-catalyzed aryl e-amination are valuable for understanding and developing new Ni-catalyzed aryl e-amination reactions and also other Ni-catalyzed electrosynthetic reactions such as C−C and C−O cross-couplings.

Introduction

Aryl amination $C(sp^2)$−N cross-coupling reactions are highly valuable and widely used in organic synthesis as aniline-type functional groups are ubiquitously present in drugs and natural products.[1-4] In 2017, Baran and co-workers reported Ni-catalyzed electrochemical aryl amination reactions (e-amination) between (hetero)aromatic halide/triflate electrophiles and aliphatic amine nucleophiles in the presence of a $NiBr_2$.DME precatalyst and 4,4'-di-tert-butyl-2,2'-dipyridyl (dtbbpy) ligand (Scheme 1).[5] Later, Baran advanced this aryl e-amination to amino acid, oligopeptides, and nucleoside nucleophiles by using bench-stable $Ni(bpy)_3Br_2$ catalyst and DBU base.[6] More recently, Rueping's group further extended the substrate scope of this aryl e-amination to electron-rich aryl halide/triflate electrophiles and weak N-nucleophiles such as aniline, sulfonamide, sulfoximine, carbamate, and imine through adjusting the strength of the base.[7] Mechanistic studies by Baran and co-workers using UV-Vis spectroscopy, electrochemical studies, and DFT calculations suggested a $Ni^{I/III}$ catalytic pathway outlined in Scheme 1.[6] In this proposed catalytic cycle, a cathodic reduction generated a $[LNi^{I}Br]$ species that directly undergoes oxidative addition with the aryl halide to form a Ni^{III} aryl intermediate, $[LNi^{III}(Ar)Br_2]$, which is rapidly transformed into a stable $[LNi^{II}(Ar)Br]$ intermediate via facile comproportionation with $[Ni^{I}]$ species or through cathodic reduction. The $[LNi^{II}(Ar)Br]$ intermediate is then converted to a Ni^{II} aryl amido complex, $[LNi^{II}(Ar)(NR_1R_2)]$, through amine ligand exchange. Anodic oxidation provides an oxidized Ni^{III} aryl amido complex $[LNi^{III}(Ar)(NR_1R_2)Br]$ for reductive elimination to produce the aryl e-amination product and recover the $[LNi^{I}Br]$ catalyst. The direct amine ligand exchange for the $[LNi^{III}(Ar)Br_2]$ intermediate to form $[LNi^{III}(Ar)(NR_1R_2)Br]$ was proposed as a minor pathway (dashed catalytic arrow in Scheme 1).

Scheme 1. Ni-Catalyzed e-Amination and Previously Proposed Mechanism.

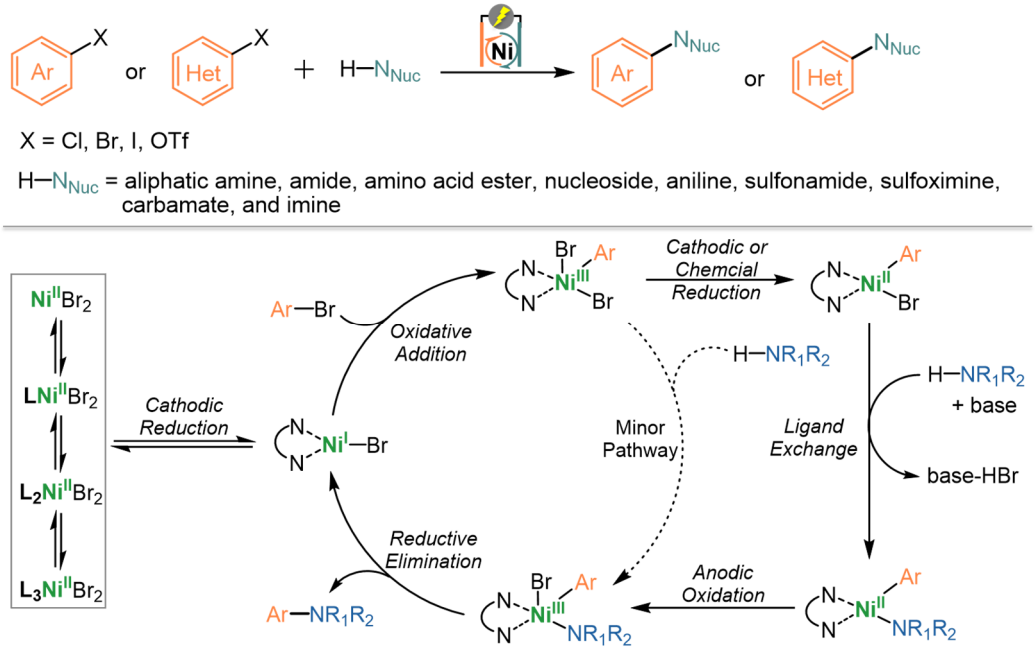

In our effort of studying mechanisms of Ni-catalyzed electrochemical C−C cross coupling reactions,[8] we serendipitously discovered that amine ligands could affect the electrochemical oxidative addition of aryl halides by Ni/bipyridine catalysts. This discovery led us to carry out comprehensive experimental and computational studies on the mechanism of Ni-catalyzed aryl e-amination reactions (Figure 1A). The combination of experiments and theory suggests a new reaction pathway where coordination of the N-nucleophile to Ni^{II} catalyst occurs before the cathodic reduction and oxidative addition steps, and the N-coordinated Ni^{II} catalyst is reduced to Ni^{I} species at the cathode through a single-electron transfer process. The Ni^{II} aryl amine intermediate is deprotonated to yield a stable Ni^{II} aryl amido intermediate, which is a key step that determines the selectivity between homo-coupling and cross-coupling reaction pathways. Experiments also suggest that bromide anion is oxidized to Br_2/Br_3^- at the anode, which not only balances the charge but also likely functions as a redox mediator to oxidize the Ni^{II} aryl amido intermediate to high-valent Ni^{III} aryl amido species for reductive elimination. These new details about the Ni-catalyzed aryl e-amination reaction will be useful for understanding and developing many other Ni-catalyzed electrosynthetic reactions such as C−O and C−C cross couplings.

Results and Discussion

Electrochemcial and Spectroscopic Studies of the Cathodically Oxidative Addition of Aryl Halide by A Ni/dtbbpy Catalyst

As a follow-up effort of our recent work on Ni-catalyzed redox-neutral electrochemical C−C cross coupling reactions,[8] we have been trying to gain a mechanistic understanding of the cathodic oxidative addition of an aryl halide by a Ni/bipyridine catalyst. To gain insight into the cathodic half-reaction of the aryl halide oxidative addition, we first conducted cyclic voltammetry (CV) studies on the reaction mixture in the negative potential range. As shown in Figure 1B, $NiBr_2$.DME/dtbbpy (1 : 1) catalyst showed a quasi-reversible redox signal with $E_{1/2}$ = -1.29 V (vs. ferrocene/ferrocenium ($Fc^{+/0}$)) (gray curve). There is no agreement on whether this redox event belongs to the single-electron transfer $Ni^{II/I}$ redox couple or the two-electron transfer $Ni^{II/0}$ redox couple.[6,8-13] We performed galvanostatic electrolysis and UV-Vis monitoring experiments on the $NiBr_2$.DME/dtbbpy (1 : 1) catalyst to reveal the electrochemical behavior of the Ni-catalyst at the cathode. As shown in Figure S1, no Ni^0 species were detected throughout the electrolysis process, even after consuming excess charges. The result suggests that the redox signal at $E_{1/2}$ = -1.29 V (vs. $Fc^{+/0}$) belongs to the $Ni^{II/I}$ redox couple.

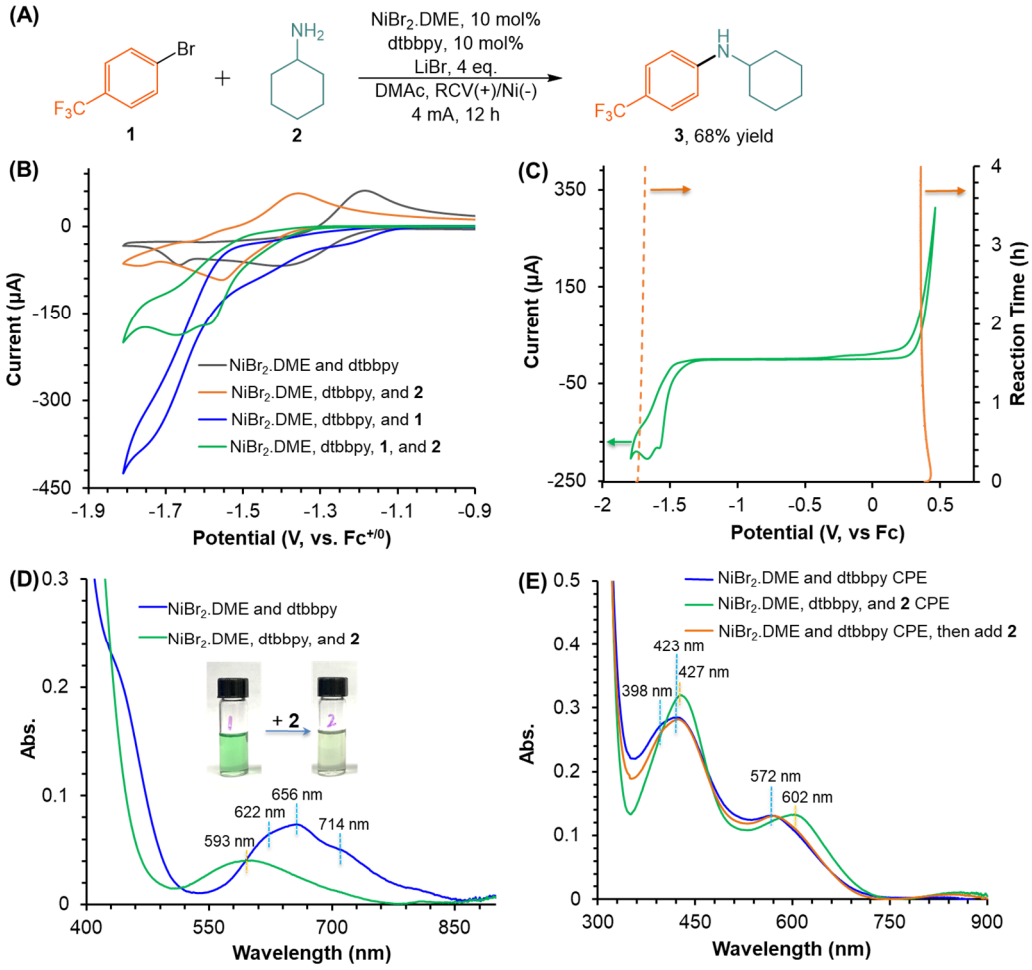

Figure 1. Ni-catalyzed e-amination and related electrochemical and UV-Vis absorption studies. (A) Ni-catalyzed e-amination reaction between 4-bromobenzotrifluoride (**1**) and NH_2Cy (**2**); (B) Cyclic voltammograms (CV) of the reaction mixtures with different combinations (scan rate, 100 mV/s and glassy carbon working electrode); (C) CV of the reaction mixture (green) and the monitored electrode potentials during the electrolysis; (D) UV-Vis spectra and photos of the Ni-catalyst in the absence (left sample, blue curve) and presence (right sample, green curve) of 30 eq. amine **2**; (E) UV-Vis absorption of the Ni^{I} species prepared through controlled potential electrolysis (CPE) of $NiBr_2$.DME/dtbbpy (1 : 1) (blue curve), a mixture of $NiBr_2$.DME/dtbbpy (1 : 1) and 30 eq. **2** (green curve), and adding 30 eq. **2** to the Ni^{I} intermediate prepared from $NiBr_2$.DME/dtbbpy (1 : 1) (orange curve).

Then we proceeded to see if an amine ligand would affect the redox chemistry of the Ni-catalyst and subsequent cathodic oxidative addition of an aryl halide. After adding cyclohexylamine (NH_2Cy, **2**), the $Ni^{II/I}$ redox signal was shifted to $E_{1/2}$ = -1.46 V (vs. $Fc^{+/0}$) (orange curve). The negative shift of redox potential is likely due to the coordination of **2** to the Ni^{II} center, as the amine is an electron-donating ligand. Further adding 4-bromobenzotrifluoride (**1**), the reductive peak current intensity was significantly increased. Meanwhile, the return peak disappeared (green curve), indicating the oxidative addition of **1** to the electrochemically generated Ni^{I} species. Notably, in the absence of **2**, the current response of Ni-catalyst to aryl bromide **1** was much stronger and the reductive onset potential was more positive (blue curve). The reduced current response of Ni-catalyst to **1**, in the presence of **2**, is likely due to the coordination of **2** to Ni^{I} species, which leads to an extra steric hindrance effect and slows down the oxidative addition reaction. As shown in Figure S2, the current response of Ni-catalyst to the aryl bromide **1** in the presence of less hindered octan-1-amine (**4**) and more hindered *tert*-butylamine (**5**) was in order of **4** > **2** > **5**.

Experimental Studies of Electrochemcial Aryl Amination by A Ni/dtbbpy Catalyst

Then, we examined the aryl e-amination reaction using **1** as an electrophile, **2** as a nucleophile, and a $NiBr_2$.DME/dtbbpy catalyst (Figure 1A). 68% yield of the amination product **3** was obtained after galvanostatic electrolysis in an undivided cell, which is comparable to previous reports.[5] A higher yield of amination product **6** (81%) was obtained from **4**. However, only 17% yield of product **7** was obtained from **5** (Scheme 2A). It shows the effect of steric hindrance of the amine substrates on the reaction efficiency. In contrast to the reported mechanism (Scheme 1) where amine coordinates with Ni after the oxidative addition of an aryl halide, our results reveal that the amine coordination with the Ni-catalyst occurs as the first step and suggests a different catalytic

mechanism of Ni-catalyzed arylamination. This observation inspired and encouraged us to examine the electrochemical arylamination in more detail.

When we prepared the reaction mixture, we noticed an apparent color change in the $NiBr_2$.DME/dtbbpy (1 : 1) catalyst from green to light yellow-green after adding **2** (picture in Figure 1D). UV-Vis spectra of the $NiBr_2$.DME/dtbbpy (1 : 1) catalyst showed two absorption peaks centered at 656 nm and 714 nm standing for the unligated $Ni^{II}Br_2$ species (ca. 26%) and a shoulder peak centered at 622 nm representing the ligated $Ni(dtbbpy)_xBr_2$ species (x = 1, 2, 3, ca. 74%), respectively (blue curve in Figure 1D, also see Figure S3 for detail). After adding **2**, a broad absorption peak centered at 593 nm was observed (green curve in Figure 1D, also see Figure S4). This shifted peak indicates the coordination of **2** to the Ni-center of both unligated $Ni^{II}Br_2$ species and ligated $Ni(dtbbpy)_xBr_2$ species which leads to electronic structure changes in the Ni^{II} complexes. M06-L[14] DFT calculations indicate that the coordination of **2** to $Ni(dtbbpy)Br_2$ is exothermic by 21.3 kcal/mol.

To understand the structure and reactivity of cathodic reduction generated Ni^{I} species, we synthesized the Ni^{I} species through control potential electrolysis (CPE) for UV-Vis studies. As shown in Figure 1E, the Ni^{I} species prepared in the presence of **2** showed two UV-Vis absorption peaks at 427 nm and 602 nm (green curve). However, UV-Vis absorption of the Ni^{I} species prepared in the absence of **2** displayed three peaks at 398 nm, 423 nm, and 572 nm (blue curve). The UV-Vis absorption difference is likely due to the coordination of amine to the Ni^{I}-center in the presence of **2**. We noticed that the Ni^{I} species prepared with and without **2** are both unstable and decompose in a few hours (Figure S5), which is consistent with the previous report.[9] The UV-Vis absorption of the Ni^{I} species prepared without **2** remained unchanged after adding 30 eq. **2** (orange curve). The results indicate that the cathodic reduction of Ni^{II} to Ni^{I} does not lead to the dissociation of the amine from the Ni^{I}-center, but the coordination of **2** to the Ni^{I}-center of pre-synthesized Ni^{I} species is unfavorable. Further studies revealed the cathodic reduction of Ni-bipyridine complex in the absence of amine yields a [Ni^{I}] tetramer,[15] which is stable to amines (Figure S6 for detail). These results strongly suggest that **2** is coordinated to the Ni-catalyst in both Ni^{II} and Ni^{I} states. This is important, because, without amine coordination, Ni^{II} aryl and Ni^{III} aryl intermediates generated from the oxidative addition of aryl bromide to low-valent Ni species (Ni^{I} and Ni^{0}) are unstable and rapidly convert to the homo-coupling biaryl product (Figure S7 – S9).

Scheme 2. Ni-Catalyzed e-Amination Using Different Amines, Anode, and Supporting Electrolytes (SE).

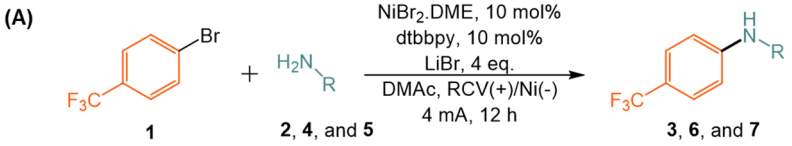

Entry	1	2	3
Amine	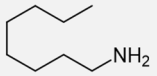 4	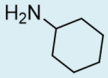 2	 5
Yield (%)	81(**6**)	68 (**3**)	17/74* (**7**)

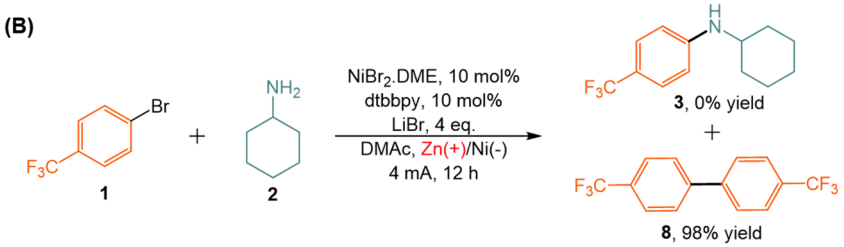

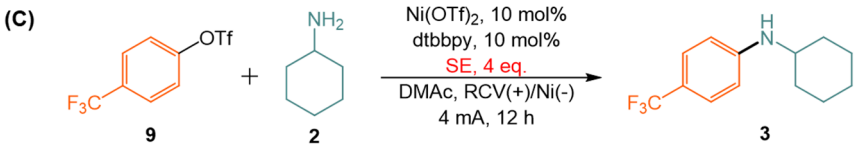

Entry	1	2	3
SE	LiBr	$LiClO_4$	$LiClO_4$ + 10 mol% Fc
Yield of **3** (%)	62	Trace**	54

*3 eq. of DBU was added. **78% yield of **8**.

As shown in Figure 1C, the CV curve of the reaction mixture displayed a cathodic peak with -1.40 V onset potential representing the Ni-catalyzed C−Br bond activation and an anodic signal with a 0.21 V (vs. $Fc^{+/0}$) onset potential standing for the Br^- anion oxidation (Figure S10). However, the Ni^{II} aryl amido intermediate displayed very weak electrochemical activity and delivered an ignorable oxidative peak with E_{peak} = -0.23 V (vs. $Fc^{+/0}$, Figure S11 and S12 for detail). Under galvanostatic electrolysis conditions, the potentials of the cathode and anode were maintained in the ranges of -1.68 – -1.70 V and 0.36 – 0.43 V (vs. $Fc^{+/0}$), respectively, which matches the redox potentials of Ni-catalyzed C−Br activation and Br^- oxidation. It demonstrates that the anodic half-

reaction is Br^- anion oxidation to Br_2/Br_3^- rather than the oxidation of the Ni^{II} aryl amido intermediate to a Ni^{III} aryl amido species, as shown in Scheme 1.

To investigate the impact of anodic half-reaction on the aryl e-amination, we conducted a control experiment using Zn metal as a sacrificial anode, in which Zn stripping instead of Br^- oxidation at the anode balances the charge (Scheme 2B). Without involving the anodic oxidation of Br^-, the aryl bromide **1** was nearly quantitatively converted into the home-coupling product, **8**. To gain insight into the function of anodic Br^- oxidation in the e-amination reaction, bromide-free 4-(trifluoromethyl)phenyl trifluoromethanesulfonate, **9**, and $Ni(OTf)_2$ were used to replace the aryl bromide **1** and $NiBr_2$.DME in the standard reaction (Scheme 2C). Using LiBr as the supporting electrolyte, **3** was produced in 62% yield (Scheme 2C, Entry 1), comparable to the standard reaction shown in Figure 1A. However, only a trace amount of **3** (< 2%) was obtained when using $LiClO_4$ as the supporting electrolyte (Scheme 2C, Entry 2). It is interesting that the yield of **3** was improved to 54% by adding 10 mol% ferrocene (Fc) (Scheme 2C, Entry 3). CV curves of these three reaction mixtures showed that electrochemical oxidation of Br^- anion (E_{onset} = 0.16 V), amine **2** (E_{onset} = 0.6 V), and Fc (E_{onset} = -0.12 V) occurred in the positive potential range, respectively (Figure S13A). Meanwhile, the cell voltage of these three reaction systems was maintained in the ranges of 2.16 – 2.31 V, 3.05 – 3.29 V, and 1.87 – 1.89 V, respectively (Figure S13B).

These results indicate that direct electrochemical oxidation of the Ni^{II} aryl amido intermediate at the anode is not favorable due to its low concentration and poor electrochemical activity. Instead, the Ni^{II} aryl amido intermediate (E_{peak} = -0.23 V, vs. $Fc^{+/0}$) is chemically oxidized to Ni^{III} aryl amido by anodically generated Br_2/Br_3^- (E_{onset} = 0.16 V, vs. Fc) or ferrocenium (Fc^+, $E_{1/2}$ = 0 V, vs. Fc) oxidant. This role of redox mediators for promoting the electrochemical oxidation of the Ni^{II} aryl amido intermediate is mechanistically important. Ni-catalyzed thermal C−N cross-couplings typically require high temperatures (> 70 °C) to drive the reductive elimination at the stage of the Ni^{II} aryl amido, representing a critical challenge for broad applications.[5] The beauty of the mediated electrochemical oxidation of the Ni^{II} aryl amido enables the formation of the Ni^{III} aryl amido intermediate, and then subsequent facile reductive elimination of the Ni^{III} aryl amido yields the C−N cross-coupling product at room temperature.

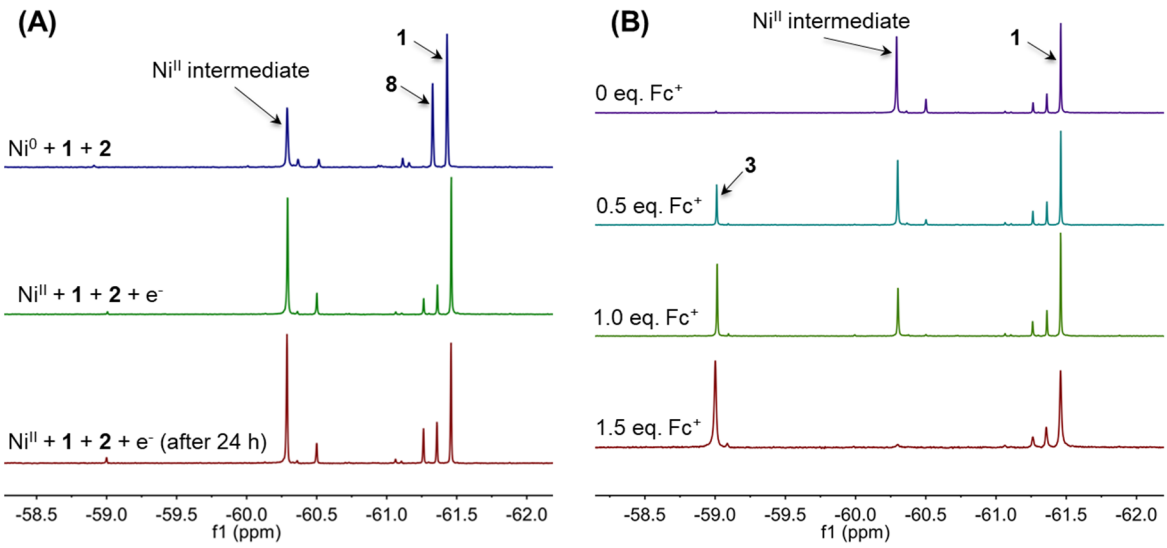

Figure 2. ^{19}F-NMR studies of the Ni^{II} aryl amido intermediate. (A) ^{19}F-NMR spectra of the chemical (blue) and electrochemically synthesized Ni^{II} aryl amido intermediate (green: fresh prepared, red: standing for 24 h); (B) Conversion of the Ni^{II} aryl amido intermediate to **3** by adding Fc^{+} oxidant. Chemical reaction conditions: **1** (54 mg, 0.24 mmol, 1.2 eq), **2** (600 mg, 6.0 mmol, 30 eq.), Ni(COD)$_2$ (55 mg, 0.2 mol, 1 eq.), dtbbpy ligand (55 mg, 0.2 mol, 1 eq.), LiBr (86 mg, 1.0 mmol), DMAc (2.5 mL), room temperature for 30 min. Electrochemical reaction conditions: **1** (54 mg, 0.24 mmol, 1.2 eq), **2** (600 mg, 6.0 mmol, 30 eq.), NiBr$_2$.DME (62 mg, 0.2 mol, 1 eq.), dtbbpy ligand (55 mg, 0.2 mol, 1 eq.), LiBr (86 mg, 1.0 mmol), DMAc (2.5 mL); Zn anode and Ni foam cathode, 5.0 mA constant current electrolysis for 1 h.

Taking advantage of the fluorine tagged 4-bromobenzotrifluoride electrophile (**1**), ^{19}F-NMR measurements were carried out to monitor the reaction at the cathode side and detect reaction intermediates. As shown in Figure 2A, ^{19}F-NMR spectra of the **1**, **2**, and [Ni^{0}] mixture delivered a peak with a chemical shift of -61.36 ppm representing the homo-coupling product **8**. The peak with a chemical shift of -60.29 ppm is assigned as an Ni^{II} aryl amido intermediate, Ni^{II}(dtbbpy)(Ar)(NHCy), which is generated from the oxidative addition of [Ni^{0}] species to **1** (blue curve). Another smaller peak at -60.52 was also observed and is assigned as an Ni^{II} aryl amine intermediate, Ni^{II}(dtbbpy)(Ar)(NH$_2$Cy)Br. When DBU was added, Ni^{II}(dtbbpy)(Ar)(NH$_2$Cy)Br could be converted to Ni^{II}(dtbbpy)(Ar)(NHCy) (Figure S14). Then, we used a Zn sacrificial anode to replace the RVC anode for galvanostatic electrolysis. Under the electrochemical conditions, the same peak of the Ni^{II} aryl amido intermediate was observed in the mixture of NiBr$_2$.DME/dtbbpy, aryl bromide **1**, and amine **2** after galvanostatic electrolysis (green curve). It proved that the Ni^{II} aryl amido intermediate is the product of the cathodic half-reaction. It is worth noting that the Ni^{II}

aryl amido intermediate is highly stable. After standing for 24 h, the ^{19}F-NMR signal at -60.29 ppm remained nearly identical (red curve).

However, in the absence of amine **2**, no Ni^{II} aryl intermediate was observed. The aryl bromide substrate was directly converted to the homo-coupling biaryl product, **8** (Figures S15). It is likely due to the trend of unstable Ni^{II} aryl species to decompose to yield the homo-coupling product (Figure S16). As shown in Figure 2B, when we added the ferrocenium tetrafluoroborate ($FcBF_4$) oxidant into the pre-prepared Ni^{II} aryl amido intermediate, Ni^{II}(dtbbpy)(Ar)(NHCy), the ^{19}F-NMR signal of the Ni^{II} aryl amido intermediate at -60.29 ppm gradually decreased, and a new peak at -59.01 ppm standing for the amination product **3** appeared through reductive elimination of the Ni^{III} aryl amido species. This observation further supports the assignment of the peak at -60.29 as the Ni^{II} aryl amido intermediate. After adding 2.0 eq. of the Fc^+ oxidant, the Ni^{II} aryl amido intermediate was fully converted to **3**. The same transformation was observed in the ^{1}H-NMR spectra (Figure S17). In contrast, upon further electrochemical reduction of the Ni^{II} aryl amido intermediate, the homo-coupling biaryl product **8** was formed (Figures S18 and S19). Kinetic studies of the oxidative addition reaction between **1** and the Ni^{I}(dtbbpy)(NH_2Cy)Br species to form the Ni^{II} aryl amido intermediate showed first-order dependence on both **1** and Ni^{I}(dtbbpy)(NH_2Cy)Br species with a small rate constant of 1.46×10^{-4} s^{-1} (Figures S20 and S21). These results indicate that the Ni^{II} aryl amido intermediate is likely the resting state of the Ni-catalyst in the reaction process, and the oxidation of the Ni^{II} aryl amido intermediate to the Ni^{III} aryl amido species is critical for the reductive elimination to selectively produce **3**. It is worth noting that both the ^{19}F-NMR and ^{1}H-NMR spectra of the Ni^{II} aryl amido intermediate appeared as sharp peaks (Figure 2 and Figure S17), indicating the diamagnetic nature of the Ni^{II}-center and a square planar structure of the Ni^{II} aryl amido intermediate.[16-19]

As shown in Scheme 2A, entry 3, the yield of the amination product **7** was significantly improved from 17% to 74% by adding 3 eq. DBU additive. ^{19}F-NMR was applied to monitor the cathodic half-reaction in the mixture of **1**, **5**, and the Ni-catalyst (Figures S22 and S23). In the absence of the DBU additive, a Ni^{II} aryl amine intermediate was detected after electrolysis for 0.5 h (Figure S22A). The Ni^{II} aryl amine intermediate is unstable and slowly converts to the homo-coupling product, **8** (Figure S22B). However, with DBU, the Ni^{II} aryl amine intermediate was deprotonated to a stable Ni^{II} aryl amido intermediate which leads to further oxidation and reductive elimination to produce the amination product **7** favorable (Figure S23 for detail). The results

strongly indicate that the deprotonation step occurs at the Ni^{II} aryl amine intermediate and that this deprotonation is a key step steering selectivity between homo-coupling and cross-coupling reaction pathways.

We also repeated the Ni-catalyzed electrochemical C−N and C−O cross-coupling reactions under the optimized conditions developed by Baran and Rueping.[6,7,20] Using $Ni(bpy)_3Br_2$ as the catalyst, DBU or Et_3N as the base, and TBABr as the supporting electrolyte, the C−N cross-coupling between aryl bromide **1** and cyclohexylamine (**2**), leucine methyl ester hydrochloride (**10**), and aniline (**12**) and the C−O cross-coupling between **1** and 2-phenylethan-1-ol (**14**) delivered 86%, 71%, 46%, and 67% yields for the products **3**, **11**, **13**, and **15**, respectively (Figure S24). The loading of the base displayed a significant effect on the reaction efficiency, as lower yields of or no cross-coupling products were detected when reducing the loading or without the addition of a base. Due to the weak coordination of aniline and alcohol, **12** and **14** don't coordinate with the Ni-catalyst in the absence of Et_3N or DBU (Figures S25 and S26). Thus, without Et_3N or DBU, only homo-coupling product **8** was obtained in the reactions between **1** and **12** or **14**. However, with the assistance of DBU and Et_3N, **12** and **14** can be efficiently deprotonated to lead the formation of the critical Ni^{II} aryl amido intermediate (Figure S25 and S26), which makes the cross-coupling favorable.

Computational Studies of Electrochemcial Aryl Amination by A Ni/dtbbpy Catalyst

M06-L calculations were used to directly evaluate the energetic impact of cyclohexylamine **2** coordination to Ni-center during cathodic reduction and subsequent aryl bromide oxidative addition and aryl amine generating reductive elimination reaction steps. Figure 3 shows the generalized potential-energy profile for **2** coordination to $Ni^{II}(dtbbpy)Br_2$ (**A**) followed by cathodic reduction and oxidative addition with the aryl bromide **1**. Consistent with the UV-Vis and CV measurements, N-coordination of **2** to triplet spin state $Ni^{II}(dtbbpy)Br_2$ (singlet **A** is 7 kcal/mol higher in enthalpy) to give **B** is exothermic by 21.3 kcal/mol. This coordination is favorable on the Gibbs energy surface and is exergonic by 8.3 kcal/mol. The singlet enthalpy of **B** is 14 kcal/mol higher than the triplet spin state. Despite the thermodynamics being stabilizing for **2** coordination, UV-Vis measurements suggested coordination to **A** is kinetically slow (Figure S4). Therefore, we examined alternative Ni^{II}–Br ground-state structures that would kinetically inhibit coordination.

The calculations suggested that dinuclear and tetranuclear Ni^{II} species are off-cycle feasible ground states (see SI) that are responsible for slow amine coordination.

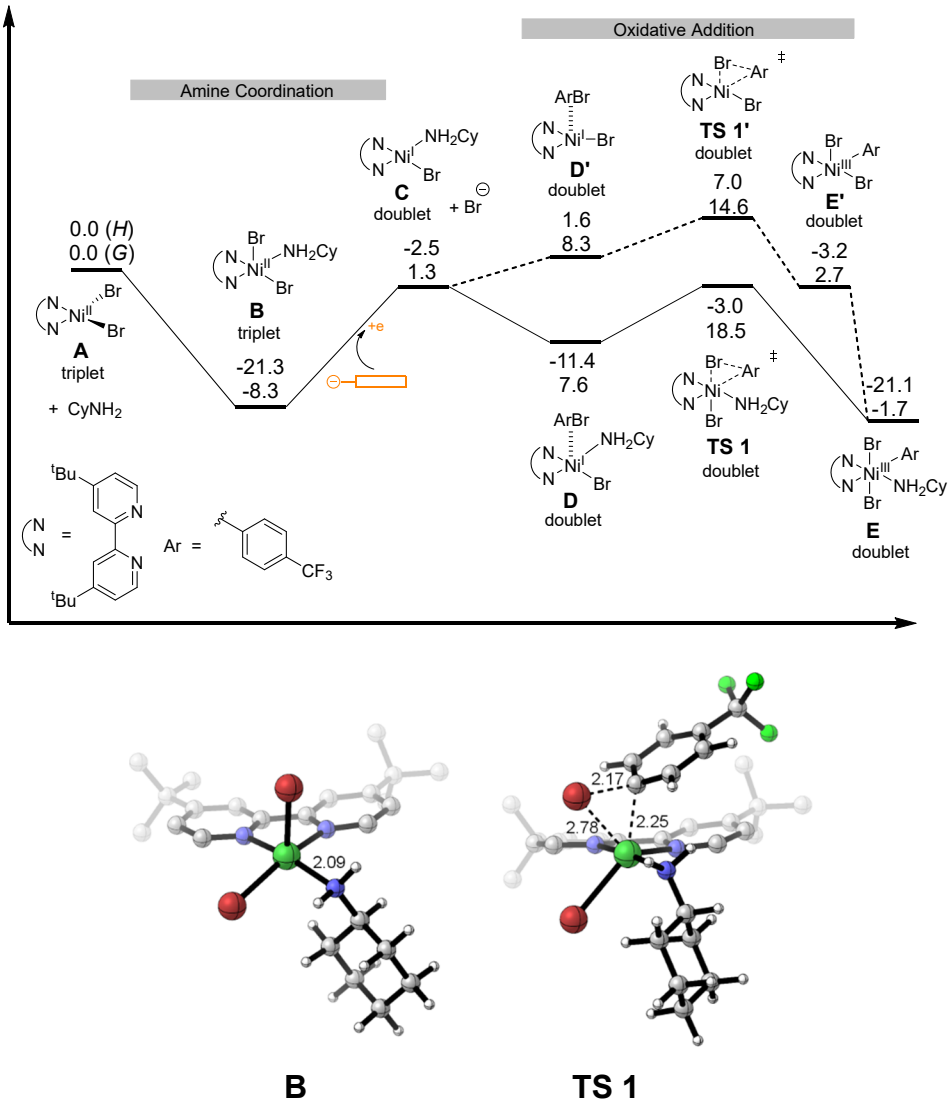

Figure 3. Top: M06-L/6-31G**|LANL2DZ[21,22] energy landscape for the Ni-catalyzed electrochemical aryl amination cross-coupling. Bottom: M06-L optimized structures. See SI for computational details.

From **B**, it is possible to compare the transition states and pathways of oxidative addition with **1**. Using the experimental cathode potential (an absolute potential = 4.9 V),[23] reduction and bromide loss give the Ni^{I} intermediate **C** that is close to the same energy as the starting Ni^{II} structure **A**. The lower energy pathway in Figure 3 shows the oxidative addition transition state **TS 1**[24] from the doublet spin Ni^{I} cyclohexylamine complex. From an initial weak charge-transfer type complex (**D**), C−Br bond cleavage through **TS 1** only requires an enthalpy change of 8

kcal/mol to give the doublet spin Ni^{III} complex **E**. Importantly, this lower energy pathway can be directly compared to the similar oxidative addition transition state **TS 1'** without **2** coordination (dotted line pathway). On the enthalpy surface **TS 1'** is 10 kcal/mol higher in energy than **TS 1**, which reflects the coordination energies of **D** and **D'**. It is noteworthy that on the Gibbs energy surface **TS 1'** is a few kcal/mol lower, but this is the result of comparing the unequal translational entropies that are likely overestimated. We also compared **TS 1** with several other alternative oxidative addition transition states, such as with extra bromide anion coordination in place of **2**. In all cases, we could not locate a lower energy oxidative addition transition state than **TS 1**. In support of the reaction pathway shown in Figure 3, we examined the coordination and oxidative addition of ethylamine and *tert*-butyl amine in comparison to **2**. Consistent with experiments and the relative spatial size of the tert-butyl group versus the cyclohexyl group and ethyl groups, there is more exothermic coordination with ethylamine and a lower barrier for oxidative addition (see SI).

From the octahedral doublet Ni^{III} intermediate **E**, we calculated several different reaction pathways that culminate in reductive elimination to form the aryl amine. We first examined the possibility that **E** undergoes a one-electron cathodic reduction and bromide loss to generate a Ni^{II}(dtbbpy)(Ar)(NH_2Cy)Br species. The thermodynamics for this reduction, as well as subsequent proton transfer to another **2** to give a Ni^{II}(dtbbpy)(Ar)(NHCy) type species, is endothermic by about 7 kcal/mol. It was surprising to find that both reduction and proton transfer steps (in either order) are not exothermic because ^{19}F-NMR indicates the formation of a Ni^{II} aryl amido intermediate, Ni^{II}(dtbbpy)(Ar)(NHCy) (see Figure 2), that is possibly a resting state. This prompted us to examine if Ni^{III} to Ni^{II} reduction occurs chemically and is stimulated by a Ni^{I} type structure, especially because ligand exchange between Ni^{II} and Ni^{III} species is significantly endothermic (see SI). We identified two exothermic reaction steps. The first involves Ni^{I}(dtbbpy)Br react with **E** to give **A** and Ni^{II}(dtbbpy)(Ar)(NH_2Cy)Br, which is 13 kcal/mol exothermic. However, this reaction is unlikely since the experiments demonstrate that, in the presence of amine **2**, the Ni^{I}(dtbbpy)Br species are not formed in the reaction system (Figure 1E). Instead, it is more likely that **C** reacts with **E** chemically to give Ni^{II}(dtbbpy)(NH_2Cy)Br_2 (**B**) and Ni^{II}(dtbbpy)(Ar)(NH_2Cy)Br (**F**), which is exothermic by 18 kcal/mol. This chemical transformation was proved by our experiments. As shown in Figures S27 and S28, a 1 : 1 ratio mixture of **1** and pre-synthesized Ni^{I}(dtbbpy)(NH_2Cy)Br (**C**) delivered about 50% yield of Ni^{II}

aryl amido intermediate (**G**). It indicates 1 eq. aryl bromide consume 2 eq. [Ni^{I}] species, where 1 eq. **C** oxidative addition with **1** to form **E**, while another 1 eq. **C** reacts to **E** through comproportionation to produce **B** and **F**. It also resulted in a Faradaic efficiency of less than 50% of the aryl e-amination reaction (Figure S31).

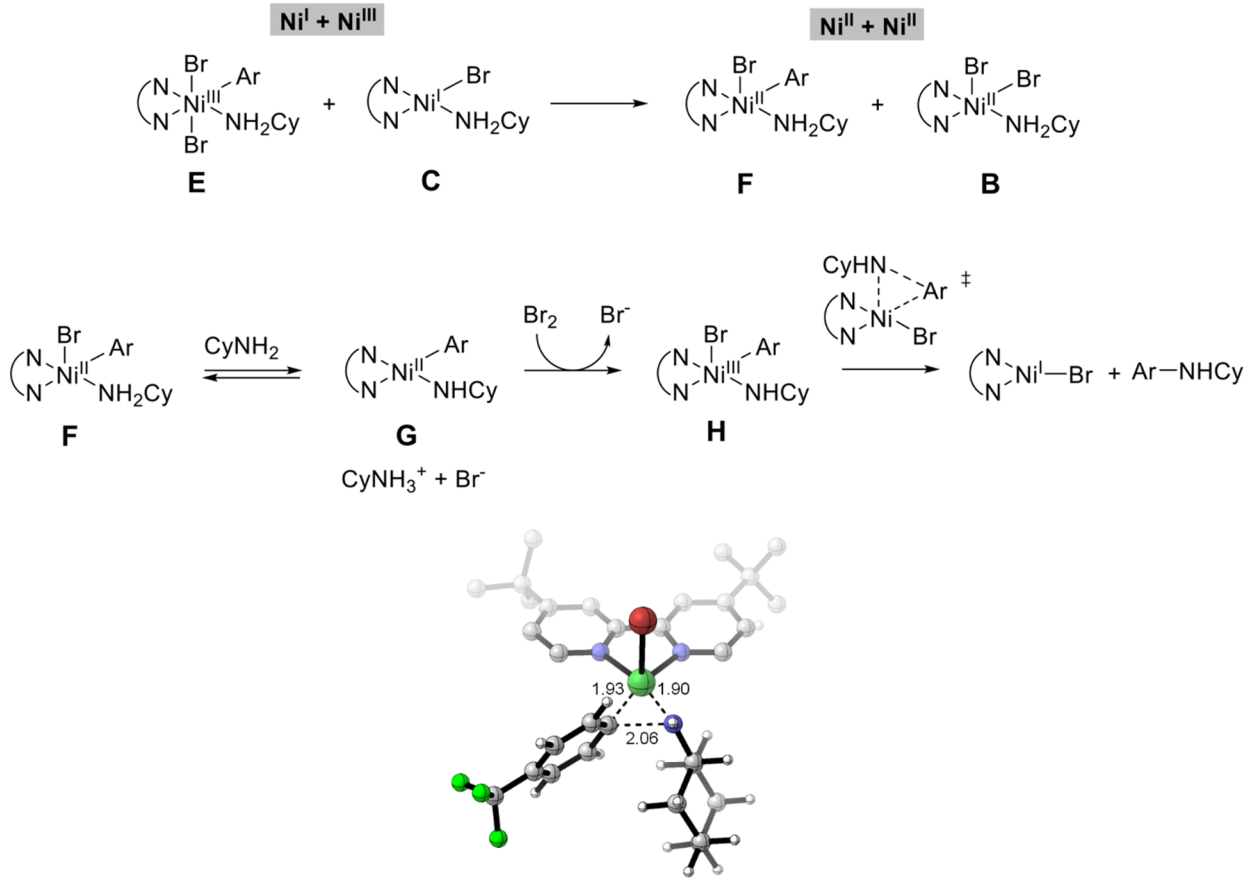

Figure 4. Top: Outline of Ni^{I}/Ni^{III} conversion to Ni^{II}. Middle: Outline of reaction pathway from Ni^{III} aryl amino intermediate **E** to aryl amination cross-coupling product. Bottom: M06-L optimized reductive elimination transition-state structure.

Deprotonation of the Ni^{II} aryl amine intermediate **F** by cyclohexylamine **2** gives the Ni^{II} aryl amido intermediate **G** (Figure 4). This intermediate is critical because it provides the pathway forward for chemical oxidation by Br_2/Br_3^- to give Ni^{III}(dtbbpy)(Ar)(NHCy)Br (**H**). We estimated the barrier for an S_N2-type transition state using a nudged elastic band method, which gave a barrier of 7 kcal/mol. The chemical oxidation to **H** provides a highly reactive Ni^{III} aryl amido intermediate that only has a 3 kcal/mol barrier for reductive elimination to generate the aryl amine product.

Importantly, the formation of the aryl amine and resulting Ni^{I}(dtbbpy)Br intermediate is exothermic by 56 kcal/mol.

Proposed Electrocatalytic Cycle for Aryl Amination by A Ni/dtbbpy Catalyst

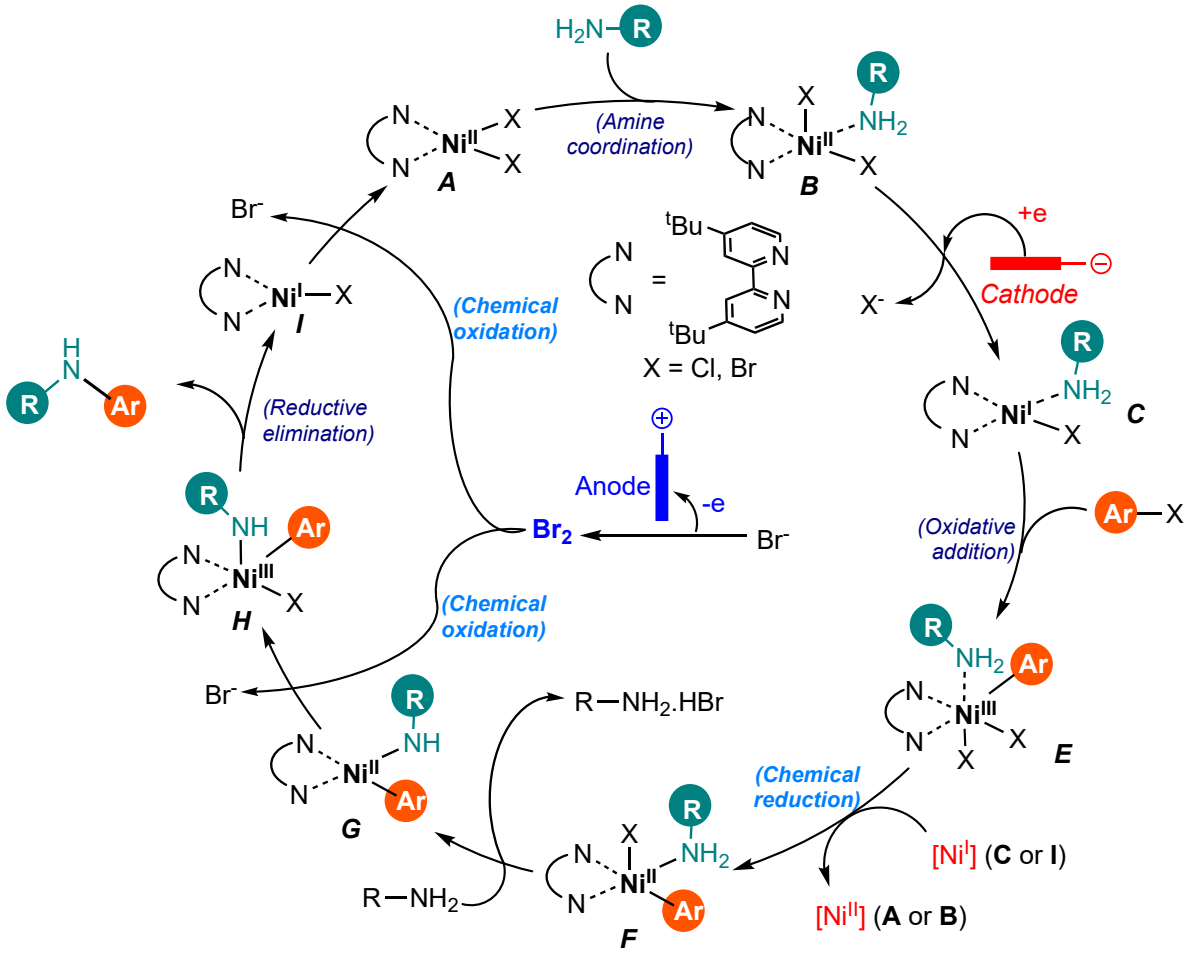

Figure 5. Proposed reaction mechanism for the Ni-catalyzed aryl e-amination reactions.

Based on the experimental and computational results presented above, a proposed complete catalytic cycle is presented in Figure 5. Amine coordinates to the Ni(dtbbpy)Br_2 catalyst (***A***) to form intermediate ***B*** when the reaction components are mixed. Then, ***B*** is reduced to Ni^{I} species ***C*** at the cathode, and then the Ni^{I} species undergoes the oxidative addition of the aryl halide to produce a high-valent Ni^{III} species ***E***. In the reaction mixture, ***E*** is rapidly chemically reduced to the Ni^{II} aryl amine complex ***F*** by Ni^{I} species (***C*** or ***I***) through comproportionation. Due to the consumption of Ni^{I} species in this step, the Faradaic efficiency of the e-amination reaction is lower than 50% throughout the duration of the reaction (Figure S31). And then, a subsequent

deprotonation step via amine base yields the stable Ni^{II} aryl amido intermediate ***G***. In the presence of bromide supporting electrolyte, intermediate ***G*** is chemically oxidized to the high-valent Ni^{III} aryl amido intermediate, ***H***, by anodically generated Br_2/Br_3^- oxidant. Reductive elimination of ***H*** produces the aryl amination product and Ni^{I} species ***I***. Finally, ***I*** is further oxidized by Br_2/Br_3^- to the intial state, ***A***, to finish the catalytic cycle. It should be noted that the direct oxidative addition of aryl halide with ***I***, as shown in Scheme 1, should be a minor pathway. As the chemical oxidation of ***I*** by Br_2/Br_3^- oxidant or Ni^{III} species is much faster than the oxidative addition reaction between ***I*** and ary halide as proved by control experiments (Figures S27-S30). Meanwhile, direct oxidative addition of ***I*** to the aryl halide substrate would lead to the formation of a homo-coupling biaryl byproduct (Figure S8 and S9).

Conclusions

In conclusion, we conducted comprehensive mechanistic studies on the reaction mechanism of the Ni-catalyzed aryl e-amination. We found that the coordination of the amine substrate to the Ni^{II}-catalyst occurs before the cathodic reduction of Ni^{II}-catalyst. In the reaction, a stable Ni^{II} aryl amido intermediate is produced from the cathodic half-reaction, which is a critical step in controlling the selectivity between cross-coupling reaction and undesired homo-coupling pathways. While at the anode side, Br^- anion is electrochemically oxidized to the Br_2/Br_3^- oxidant, which funcitions a redox mediator to chemically oxidize the Ni^{II} aryl amido intermediate to high-valent Ni^{III} aryl amido for facile reductive elimination at room temperature. The presented new insighs of the Ni-catalyzed aryl e-amination will provide valuable mechanistic guidance for understanding and developing new Ni-catalyzed aryl e-amination reactions and other Ni-catalyzed electrosynthetic reactions such C−O and C−C cross-couplings, including optimizing reaction conditions, selectively generating reactive intermediates, and avoiding undesired homo-couping.

Supporting Information contains additional experimental details and figures and tables. Supporting Information is available online or from the author.

Acknowledgements We thank the National Institutes of Health (grant no. R15GM143721) and National Science Foundation (grant no. 1847674) for supporting this study. We acknowledge that the NMR studies are supported by NSF's MRI program (award number 1429195).

References:

(1) Brown, D. G.; Boström, J. Analysis of Past and Present Synthetic Methodologies on Medicinal Chemistry: Where Have All the New Reactions Gone? *Journal of Medicinal Chemistry* **2016**, *59*, 4443-4458.

(2) Ruiz-Castillo, P.; Buchwald, S. L. Applications of Palladium-Catalyzed C–N Cross-Coupling Reactions. *Chemical Reviews* **2016**, *116*, 12564-12649.

(3) Beletskaya, I. P.; Cheprakov, A. V. The Complementary Competitors: Palladium and Copper in C–N Cross-Coupling Reactions. *Organometallics* **2012**, *31*, 7753-7808.

(4) Fischer, C.; Koenig, B. Palladium- and copper-mediated N-aryl bond formation reactions for the synthesis of biological active compounds. *Beilstein journal of organic chemistry* **2011**, *7*, 59-74.

(5) Li, C.; Kawamata, Y.; Nakamura, H.; Vantourout, J. C.; Liu, Z.; Hou, Q.; Bao, D.; Starr, J. T.; Chen, J.; Yan, M.; Baran, P. S. Electrochemically Enabled, Nickel-Catalyzed Amination. *Angewandte Chemie International Edition* **2017**, *56*, 13088-13093.

(6) Kawamata, Y.; Vantourout, J. C.; Hickey, D. P.; Bai, P.; Chen, L.; Hou, Q.; Qiao, W.; Barman, K.; Edwards, M. A.; Garrido-Castro, A. F.; deGruyter, J. N.; Nakamura, H.; Knouse, K.; Qin, C.; Clay, K. J.; Bao, D.; Li, C.; Starr, J. T.; Garcia-Irizarry, C.; Sach, N.; White, H. S.; Neurock, M.; Minteer, S. D.; Baran, P. S. Electrochemically Driven, Ni-Catalyzed Aryl Amination: Scope, Mechanism, and Applications. *Journal of the American Chemical Society* **2019**, *141*, 6392-6402.

(7) Zhu, C.; Kale, A. P.; Yue, H.; Rueping, M. Redox-Neutral Cross-Coupling Amination with Weak N-Nucleophiles: Arylation of Anilines, Sulfonamides, Sulfoximines, Carbamates, and Imines via Nickelaelectrocatalysis. *JACS Au* **2021**, *1*, 1057-1065.

(8) Luo, J.; Hu, B.; Wu, W.; Hu, M.; Liu, T. L. Nickel-Catalyzed Electrochemical C(sp3)−C(sp2) Cross-Coupling Reactions of Benzyl Trifluoroborate and Organic Halides**. *Angew. Chem. Int. Ed.* **2021**, *60*, 6107-6116.

(9) Till, N. A.; Oh, S.; MacMillan, D. W. C.; Bird, M. J. The Application of Pulse Radiolysis to the Study of Ni(I) Intermediates in Ni-Catalyzed Cross-Coupling Reactions. *J. Am. Chem. Soc.* **2021**, *143*, 9332-9337.

(10) Sandford, C.; Edwards, M. A.; Klunder, K. J.; Hickey, D. P.; Li, M.; Barman, K.; Sigman, M. S.; White, H. S.; Minteer, S. D. A synthetic chemist's guide to electroanalytical tools for studying reaction mechanisms. *Chem. Sci.* **2019**, *10*, 6404-6422.

(11) Amatore, C.; Azzabi, M.; Calas, P.; Jutand, A.; Lefrou, C.; Rollin, Y. Absolute determination of electron consumption in transient or steady state electrochemical techniques. *Journal of Electroanalytical Chemistry and Interfacial Electrochemistry* **1990**, *288*, 45-63.

(12) Duñach, E.; Franco, D.; Olivero, S. Carbon−Carbon Bond Formation with Electrogenerated Nickel and Palladium Complexes. *European Journal of Organic Chemistry* **2003**, *2003*, 1605-1622.

(13) Lu, J.; Wang, Y.; McCallum, T.; Fu, N. Harnessing Radical Chemistry via Electrochemical Transition Metal Catalysis. *iScience* **2020**, *23*, 101796.

(14) Zhao, Y.; Truhlar, D. G. A new local density functional for main-group thermochemistry, transition metal bonding, thermochemical kinetics, and noncovalent interactions. *J. Chem. Phys.* **2006**, *125*, 194101.

(15) Ting, S. I.; Williams, W. L.; Doyle, A. G. Oxidative Addition of Aryl Halides to a Ni(I)-Bipyridine Complex. *Journal of the American Chemical Society* **2022**.

(16) Qamar, O. A.; Cong, C.; Ma, H. Solid state mononuclear divalent nickel spin crossover complexes. *Dalton Transactions* **2020**, *49*, 17106-17114.

(17) Ting, S. I.; Garakyaraghi, S.; Taliaferro, C. M.; Shields, B. J.; Scholes, G. D.; Castellano, F. N.; Doyle, A. G. 3d-d Excited States of Ni(II) Complexes Relevant to Photoredox Catalysis: Spectroscopic Identification and Mechanistic Implications. *Journal of the American Chemical Society* **2020**, *142*, 5800-5810.

(18) Dommaschk, M.; Schütt, C.; Venkataramani, S.; Jana, U.; Näther, C.; Sönnichsen, F. D.; Herges, R. Rational design of a room temperature molecular spin switch. The light-driven coordination induced spin state switch (LD-CISSS) approach. *Dalton Transactions* **2014**, *43*, 17395-17405.

(19) Lin, Q.; Diao, T. Mechanism of Ni-Catalyzed Reductive 1,2-Dicarbofunctionalization of Alkenes. *Journal of the American Chemical Society* **2019**, *141*, 17937-17948.

(20) Zhang, H.-J.; Chen, L.; Oderinde, M. S.; Edwards, J. T.; Kawamata, Y.; Baran, P. S. Chemoselective, Scalable Nickel-Electrocatalytic O-Arylation of Alcohols. *Angew. Chem. Int. Ed.* **2021**, *60*, 20700-20705.

(21) Ditchfield, R.; Hehre, W. J.; Pople, J. A. Self‐Consistent Molecular‐Orbital Methods. IX. An Extended Gaussian‐Type Basis for Molecular‐Orbital Studies of Organic Molecules. *J. Chem. Phys.* **1971**, *54*, 724-728.

(22) Hay, P. J.; Wadt, W. R. Ab initio effective core potentials for molecular calculations. Potentials for the transition metal atoms Sc to Hg. *J. Chem. Phys.* **1985**, *82*, 270-283.

(23) Namazian, M.; Lin, C. Y.; Coote, M. L. Benchmark Calculations of Absolute Reduction Potential of Ferricinium/Ferrocene Couple in Nonaqueous Solutions. *Journal of Chemical Theory and Computation* **2010**, *6*, 2721-2725.

(24) Note that this **TS 1** is ~15 kcal/mol lower than the transition state reported by Baren et al., which does not have the aryl bromide in the lowest energy conformation.